

# A physical model for the redshift evolution of high- $z$ Lyman-Break Galaxies

Charles Jose<sup>1\*</sup>, Raghunathan Srianand<sup>1†</sup> and Kandaswamy Subramanian<sup>1‡</sup>

<sup>1</sup>*IUCAA, Post Bag 4, Pune University Campus, Ganeshkhind, Pune 411007, India*

9 February 2019

## ABSTRACT

We present a galaxy formation model to understand the evolution of stellar mass ( $M_*$ ) - UV luminosity relations, stellar mass functions and specific star formation rate (sSFR) of Lyman Break Galaxies (LBGs) along with their UV luminosity functions in the redshift range  $3 \leq z \leq 8$ . Our models assume a physically motivated form for star formation in galaxies and model parameters are calibrated by fitting the observed UV luminosity functions (LFs) of LBGs. We find the fraction of baryons that gets converted into stars remains nearly constant for  $z \geq 4$  but shows an increase for  $z < 4$ . However, the rate of converting baryons into stars does not evolve significantly in the redshift range  $3 \leq z \leq 8$ . Our model further successfully explains the  $M_*$  - UV luminosity ( $M_{AB}$ ) correlations of LBGs. While our model predictions of stellar mass functions compare well with the inferred data from observations at the low mass end, we need to invoke the Eddington bias to fit the high mass end. At any given redshift, we find the sSFR to be constant over the stellar mass range  $5 \times 10^8 - 5 \times 10^9 M_\odot$  and the redshift evolution of sSFR is well approximated by a form  $(1+z)^{2.4}$  for  $3 \leq z \leq 8$  which is consistent with observations. Thus we find that dark matter halo build up in the  $\Lambda$ CDM model is sufficient to explain the evolution of UV LFs of LBGs along with their  $M_*$  -  $M_{AB}$  relations, the stellar mass functions and the sSFR for  $3 \leq z \leq 8$ .

**Key words:** cosmology: theory – cosmology: large-scale structure of universe – galaxies: formation – galaxies: high-redshift – galaxies: luminosity function – galaxies: evolution

## 1 INTRODUCTION

Understanding the formation and evolution of Lyman Break Galaxies (LBGs) in the frame work of  $\Lambda$ CDM cosmology is currently a very active area of research in extragalactic astronomy. In particular understanding how various physical processes affect the star formation in individual galaxies hosted by different dark matter halos is very important for understanding galaxy evolution over cosmic time. Additionally star formation activity in high redshift galaxies influences physical conditions in the intergalactic medium through ionization, mechanical and chemical feedback. In principle various parameters of the model can be constrained by direct observables like luminosity function and clustering of LBGs and Lyman- $\alpha$  emitters (LAEs) measured at different redshifts. Models constrained by such observations can

also predict several quantities derived from observations like star formation rate (SFR), sSFR, stellar mass functions etc.

On the observational side, the past decade has witnessed an ever growing data based on UV, optical and near Infrared deep images and high resolution spectra of high redshift galaxies. The Lyman break color selection technique (Madau et al. 1996; Steidel et al. 1996; Adelberger et al. 1998; Steidel et al. 1998) enabled the detection of a substantial number of faint high redshift galaxies from various deep field surveys (Steidel et al. 1999; Giavalisco et al. 2004; Ouchi et al. 2004a; Beckwith et al. 2006; Grogin et al. 2011a; Illingworth et al. 2013) which has resulted in estimates of UV luminosity functions (LF) of the LBGs up to  $z \sim 10$  (Bouwens et al. 2007, 2008; Reddy et al. 2008; McLure et al. 2013; Schenker et al. 2013; Oesch et al. 2013; Lorenzoni et al. 2013) and also their clustering up to  $z = 5$  (Giavalisco & Dickinson 2001; Ouchi et al. 2004b, 2005; Kashikawa et al. 2006; Hildebrandt et al. 2009; Savoy et al. 2011; Bielby et al. 2011). Further, recent advances in multi-band deep field observations (Giavalisco et al. 2004; Bouwens et al. 2010; Oesch et al. 2010; Bouwens et al. 2011; Windhorst et al. 2011; Gro-

\* charles@iucaa.ernet.in

† anand@iucaa.ernet.in

‡ kandu@iucaa.ernet.in

gin et al. 2011b; Koekemoer et al. 2011) have allowed one to infer various intrinsic quantities of LBGs including their age, dust content,  $M_*$  and sSFR using Spectral Energy distribution (SED) fitting analysis (Stark et al. 2009; González et al. 2011; Reddy et al. 2012; Wilkins et al. 2012; González et al. 2014; Bouwens et al. 2012). Such a wealth of observations combined with theoretical models of galaxy formation provide a unique opportunity to probe the connection between early galaxies and dark matter halos hosting them.

We have been constructing physically motivated models to explain the LFs and clustering of LBGs and LAEs (Samui et al. 2007, 2009; Jose et al. 2013b,a) in the framework of  $\Lambda$ CDM cosmology. In our models, we assume that galaxies are formed in dark matter halos that sustain continuous star formation spreading over few dynamical time scales of the halo. The SFR is then combined with the dark matter halo formation rate to obtain the UV LF of high redshift LBGs. We have constrained the parameters related to star formation by comparing the model predictions of UV LFs of LBGs with observed data. This simple approach explains the connection between LBGs and LAEs at  $z \geq 3$  and also with the dark matter halos hosting them (Jose et al. 2013b,a). Our model is also used to understand the galactic outflows (Samui et al. 2008) and to place an independent constraint on neutrino mass (Jose et al. 2011).

While the UV luminosity of high- $z$  galaxies depends on the instantaneous SFR, the other derived quantities depend on the entire star formation history. Therefore, it is interesting to see how our models, constrained only by the UV luminosity functions at different  $z$ , predict parameters related to high- $z$  galaxies, derived using SED fitting analysis. In this paper, we investigate further to see whether our model of galaxy formation with minimal assumptions can capture the basic trends derived from SED fitting analysis. We show that, within the uncertainties in the quantities derived using SED fitting analysis, our models successfully explain various known trends such as the  $M_* - M_{AB}$  correlations, the evolution of sSFR and the stellar mass functions of LBGs at  $z \geq 3$ .

The organization of this paper is as follows. In the next section we describe our basic star formation model. In section 3 we calibrate our model parameters using the recently updated UV LF of LBGs. In section 4 we further predict the  $M_* - M_{AB}$  correlations, sSFR and stellar mass functions, compare these quantities with observations and discuss the implications. We present our conclusions in the final section. For all calculations we adopt a flat  $\Lambda$ CDM universe with cosmological parameters consistent with 7 year Wilkinson Microwave Anisotropy Probe (WMAP7) observations (Larson et al. 2011) with  $\Omega_m = 0.27$ ,  $\Omega_\Lambda = 0.73$ ,  $\Omega_b = 0.045$ ,  $h = 0.71$ ,  $n_s = 0.963$  and  $\sigma_8 = 0.801h^{-1}\text{Mpc}$ . Here  $\Omega_i$  is the background density of any species 'i' in units of critical density  $\rho_{crit}$ . The Hubble constant is  $H_0 = 100h \text{ km s}^{-1} \text{ Mpc}^{-1}$ .

## 2 THE STAR FORMATION MODEL

In Samui et al. (2007) (hereafter SSS07) we have developed a physically motivated model to explain the LFs of high redshift LBGs. The crucial component of this model (see SSS07 for more details) is that the SFR ( $\dot{M}_{SF}$ ) in a dark

matter halo of mass  $M$  collapsed at redshift  $z_c$  and observed at redshift  $z$  and is given by (Gnedin 1996; Chiu & Ostriker 2000; Choudhury & Srianand 2002)

$$\dot{M}_{SF}(M, z, z_c) = f_* \left( \frac{\Omega_b}{\Omega_m} M \right) \frac{T}{\kappa^2 t_{d(z_c)}^2} \times \exp \left[ -\frac{T}{\kappa t_{d(z_c)}} \right]. \quad (1)$$

Here,  $f_*$  is the fraction of baryons converted into stars over the life time of a galaxy and  $\kappa$  fixes the duration of this star formation activity. Also  $T = t(z) - t(z_c)$ , with  $t(z)$  being the age of the universe at redshift  $z$ , is the age of the galaxy at  $z$  is  $t(z) - t(z_c)$ . Further,  $t_d(z_c)$  is the dynamical time scale of a halo collapsing at  $z_c$  (see Eq. (3) of SSS07).

Such a functional form for the SFR in our model could be reasonable in the following way. The SFR in a halo is proportional to the available cold gas. The gas in a halo is heated to the virial temperature of the halo at the time of its collapse. Stars are formed after the cooling of this gas by radiative recombination. Thus, as the available cold gas increases with time, the SFR in that halo also increases. The linear increase in the SFR captures this phase of star formation. Eventually, the amount of cold gas (and hence the SFR) in a halo decreases because the gas gets locked into the previous stars or due to supernova feedback of earlier star formation. This could give rise to the exponential decrease in SFR. As discussed above we have shown that the star formation history given by Eq. 1, reproduces various observed properties of LBGs (See also, Samui 2014).

The star formation in a dark matter halo is affected by various feedback processes. In our models we include feedback processes related to the cooling efficiency of the gas and active galactic nuclei (AGN) activity. We assume that the gas can cool (due to recombination line cooling from hydrogen and helium) and collapse to form stars in halos with virial temperatures ( $T_{vir}$ ) greater than  $10^4$  K. However, after reionization, the photo ionization of the IGM increases the temperature of the gas thereby increasing the Jean's mass for collapse. In such regions, we incorporate the radiative feedback by complete suppression of star formation in halos with circular velocity  $v_c \leq 35 \text{ km s}^{-1}$  and no suppression in halos with circular velocity  $v_c \geq 95 \text{ km s}^{-1}$ . Further, for halos with intermediate circular velocities ( $35 \text{ km s}^{-1} \leq v_c \leq 95 \text{ km s}^{-1}$ ) a linear fit from 0 to 1 is taken as the suppression in star formation (Bromm & Loeb 2002; Benson et al. 2002; Dijkstra et al. 2004). Additionally, in our models the AGN feedback suppresses the star formation in high mass halos by a factor  $[1 + (M/M_{agn})]^{-1/2}$  (Jose et al. 2013b), where the characteristic mass scale  $M_{agn}$ , is believed to be  $\sim 10^{12} M_\odot$  (Bower et al. 2006; Best et al. 2006).

Since reionization leads to a feed back on the star formation, one should model both the star formation and reionization simultaneously in a self consistent manner. However, comparison of various predictions of our models with observations shows that the exact nature and redshift of reionization does not change these predictions in the redshift range currently probed by observations, provided the redshift reionization,  $z_{re}$ , is larger than about 8. Therefore, for applying radiative feedback, we assume a sudden reionization of the Universe at  $z_{re} = 10$ , consistent with the WMAP7 observations (Larson et al. 2011).

In summary reionization and AGN feedbacks suppresses the SFR in a given halo of mass  $M$  by a factor

$$F_s(M) = \begin{cases} \frac{1}{\left(1 + \frac{M}{M_{agn}}\right)^{\frac{1}{2}}} & v_c(M) > v_c^m \\ \frac{1}{\left(1 + \frac{M}{M_{agn}}\right)^{\frac{1}{2}}} \frac{v_c^m - v_c(M)}{v_c^m - 35} & v_c^m \geq v_c(M) > 35 \\ 0. & v_c(M) < 35 \end{cases} \quad (2)$$

where  $v_c$  is in units of  $\text{km s}^{-1}$ , so that the final star formation rate is given by  $\dot{M}_{SF}(M) \times F_s(M)$ . In our fiducial model, as discussed above, we have adopted  $v_c^m$  to be  $95 \text{ km s}^{-1}$  as suggested by Bromm & Loeb (2002).

Given the SFR from Eq. (1) one can obtain the total  $M_*$  of a galaxy at any redshift  $z$  by integrating SFR from it's collapse redshift  $z_c$  to the observed redshift  $z$ . Thus the total  $M_*$  in a galaxy that has formed at  $z_c$  and observed at  $z$  is given by

$$M_*(M, T) = f_* M \frac{\Omega_b}{\Omega_m} \left[ 1 - e^{-\frac{T}{\kappa t_d}} \left( 1 + \frac{T}{\kappa t_d} \right) \right] \times F_s(M). \quad (3)$$

The total  $M_*$  of a galaxy at any redshift  $z$ , is a function of the mass  $M$  of the host dark matter halo, it's age and the efficiency parameter  $f_*$ . From the Eq. (3) it is clear that galaxies of different age (forming at different redshifts), hosted by dark matter halos of different masses can have the same  $M_*$  at any given time of observation. This, as we see in next section, naturally introduces a scatter in various scaling relations involving  $M_*$ .

Another quantity of great interest is the specific star formation rate (sSFR), which is the instantaneous star formation rate in a galaxy per unit stellar mass in it or simply the SFR divided by the  $M_*$ . Using Eq. (1) and Eq. (3) we can compute the sSFR of a galaxy at  $z$ , which has formed at  $z_c$  as

$$sSFR(T(z, z_c)) = \frac{T/(\kappa t_d)^2}{\left[ \exp\left(\frac{T}{\kappa t_d}\right) - \left(1 + \frac{T}{\kappa t_d}\right) \right]}. \quad (4)$$

Thus in our model sSFR of a galaxy is not a function of  $f_*$  or halo mass but depends only on it's age and the duration of star formation. Therefore all the galaxies forming at the same redshift will have the same sSFR at a given redshift of observation, independent of their halo mass. However, galaxies forming at two different redshifts can have very different sSFR at a given redshift of observation. Further, sSFR decreases with the age of the galaxy, thereby younger galaxies forming close to the redshift of observation tend to posses a higher sSFR.

In order to make predictions of various derived quantities like stellar mass functions and average sSFR, we need to calibrate our model parameters, especially  $f_*$ . To do this we compare our model predictions of UV LFs of LBGs with their observed LFs over wide  $z$  range. We discuss this in the next section.

### 3 CALIBRATING THE MODEL PARAMETERS USING UV LFS OF LBGs

As in our previous work we constrain our model parameters by fitting the observed UV LFs of LBGs. Here, we briefly

describe how to compute the LFs in our models using the SFR given in Eq. (1). We first note that the halo mass and time of collapse are input parameters for Eq. (1). For any observed  $z$ , we compute the SFR for the whole range of halo masses that collapsed at different collapse redshifts  $z_c > z$ . The number density of such halos of mass  $M$  formed at  $z_c$  and observed at  $z$  is calculated from the redshift derivative of halo mass functions (see below). During the period from  $z_c$  to  $z$ , the SFR(t) in a such halo of mass  $M$  is given by Eq. (1) which is then used to compute the UV luminosity of LBGs.

For computing galaxy luminosities, we assume that stars formed with a Salpeter IMF in the mass range  $0.1 - 100 M_\odot$ . This is very much similar to what is used by the observers to interpret their data. We use the population synthesis code STARBURST99 (Leitherer et al. 1999) to obtain the rest frame luminosity ( $l_{1500}$ ) at  $1500 \text{ \AA}$ , as a function of time of a galaxy undergoing a burst of star formation. The luminosity of a galaxy ( $L_{1500}$ ) is obtained by convolving the SFR given by Eq. (1) with this burst luminosity at  $1500 \text{ \AA}$ ,

$$L_{1500}(T) = \int_T^0 \dot{M}_{SF}(T - \tau) l_{1500}(\tau) d\tau. \quad (5)$$

The observed luminosity is reduced to a fraction,  $1/\eta$ , of  $L_{1500}$  due to the dust absorption in the galaxy, thus the observed luminosity is  $L_{1500}/\eta$ . This luminosity ( $L_0 = L_{1500}/\eta$ ) is then converted to a standard absolute AB magnitude  $M_{AB}$ , using

$$M_{AB} = -2.5 \log_{10}(L_0) + 52.60 \quad (6)$$

where the luminosity is in units of  $\text{erg s}^{-1} \text{ Hz}^{-1}$  (Oke & Gunn 1983). Knowing  $M_{AB}$  of individual galaxies we then compute the LF,  $\Phi(M_{AB}, z)$ , at a given redshift  $z$  using,

$$\begin{aligned} \Phi(M_{AB}, z) dM_{AB} &= \int_z^\infty dz_c \frac{d^2 n}{dM dz_c} (M(M_{AB}), z_c) \frac{dM}{dL_{1500}} \\ &\times \frac{dL_{1500}}{dM_{AB}} dM_{AB}. \end{aligned} \quad (7)$$

Here,

$$\frac{d^2 n}{dM dz_c} (M, z_c) = \frac{dt}{dz_c} \frac{d\dot{n}}{dM} (M, z_c) \quad (8)$$

where  $\frac{d\dot{n}}{dM} (M, z_c)$  is the formation rate of halos in the mass range  $(M, M + dM)$  at redshift  $z_c$ . SSS07 found that using the time derivative of Sheth & Tormen (1999) (hereafter ST) mass functions reproduces the observed LF of high- $z$  LBGs very well. Therefore we use  $\frac{d\dot{n}}{dM} (M, z_c) = \frac{d}{dt} \frac{dn_{ST}}{dM} (M, z_c)$  with  $\frac{dn_{ST}}{dM} (M, z_c)$  being the ST mass function at  $z_c$ .

In our fiducial model we have chosen  $\kappa = 1.0$  at all redshifts as it is consistent with the LF (SSS07) and the clustering (Jose et al. 2013b) studies. Thus the characteristic time scale for star formation is set to the dynamical time scale of the halo. We also varied  $M_{agn}$ , the parameter controlling the AGN feedback, at each redshift to obtain the best fit LFs. The best fit  $M_{agn}$  values are found to be  $5.5 \times 10^{11}$  and  $1.6 \times 10^{12} M_\odot$  at redshifts 3 and 4 in our models. In addition we find that our model does not require any AGN feedback to reproduce the observed LF for  $z = 5 - 8$ . This is mainly due to the lack of accurate LF measurements in the high luminosity end in these redshifts. We also note that

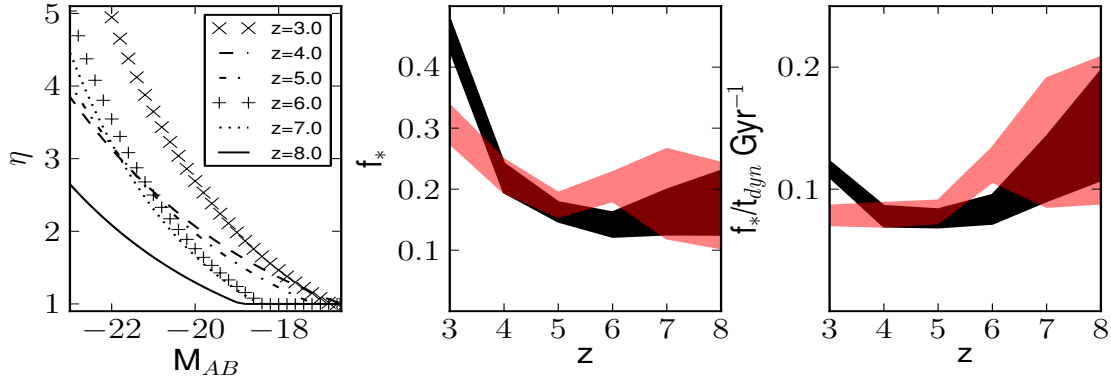


**Figure 1.** Left: The best fit dust correction parameter given by Bouwens et al. (2009, 2012) as a function of the absolute AB magnitude for redshifts 3 – 7. Middle and right panels respectively show the  $1\sigma$  range of  $f_*$  and  $f_*/t_d$  as a function of redshift, obtained by fitting our model predictions of UV LF with the observed data. Here the shaded black (dark) region and shaded red (grey) region are for our fiducial models A and B (see section 3) respectively.

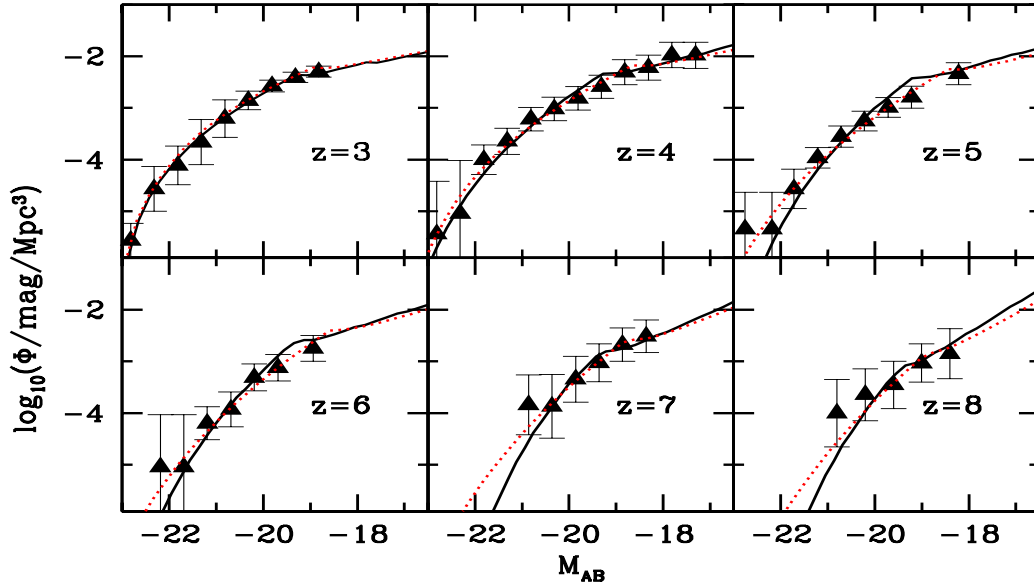


**Figure 2.** Comparison of observed UV LF of LBGs at different redshifts with our best fit model predictions. The observed data points and error bars are from Reddy et al. (2008) (for  $z = 3$ ) and Bouwens et al. (2007) (for  $z = 4 - 7$ ). We take cosmic variance into account by adding an uncertainty of 14 % into Poisson error in quadrature for  $z \geq 4$  (Bouwens et al. 2007). The solid black lines corresponds to model A where we apply luminosity dependent dust correction and red dotted lines corresponds to model B where luminosity independent dust correction is applied.

fixing AGN feedback mass scale to be  $10^{12} M_\odot$  at all the redshifts also provide a reasonable fit to the UV LFs at those redshifts. Thus the evolution of AGN feedback parameter is not essential for our models.

We use the dust extinction parameter,  $\eta$ , determined by a number of recent studies. These studies, using SED fitting analysis, derive (i)  $\eta$  as function of the luminosity at a given redshift and (ii) the average luminosity function weighted  $\eta$  for different redshifts (Stark et al. 2009; Reddy & Steidel 2009; Bouwens et al. 2009, 2012; Reddy et al. 2012).

Therefore, at any redshift we consider two fiducial models A and B; in model A we use the luminosity dependent  $\eta$  and in model B, the luminosity function weighted average  $\eta$ .

The luminosity dependent  $\eta$  for model A is computed using the recent estimates of UV-continuum slope  $\beta$  from Bouwens et al. (2012). The dust extinction ( $\eta$ ) is related to UV-continuum slope through the IRX- $\beta$  relation  $2.5 \log_{10}(\eta) = 4.43 + 1.99\beta$  (Meurer et al. 1999). Using SED fitting analysis, Bouwens et al. (2012) provides  $\beta$  as a function of the UV magnitude  $M_{AB}$  in the redshift range 4–7 (see

Table 5 of their paper). In this work, we use the values of  $\beta$  and  $d\beta/dM_{AB}$  at  $M_{AB} = -19.5$  given by Bouwens et al. (2012) and obtain UV-continuum slope at other magnitudes by assuming a linear relation between  $\beta$  and  $M_{AB}$ . Further, for redshifts 3 and 8, where observational data is not available we use  $\beta$  and  $d\beta/dM_{AB}$ , extrapolated from other  $z$ . The values of  $\beta$  and  $d\beta/dM_{AB}$  at  $M_{AB} = -19.54$  are also given in Table 1. The luminosity dependent  $\eta$  computed in this way for different  $z$  is plotted in the left panel of Fig. 1 (see also Fig. 14 of Bouwens et al. 2012). The average  $\eta$  used in our model B is taken from Bouwens et al. (2009) for  $z = 3$  and Bouwens et al. (2012) for  $z = 4 - 7$  (see Table 6 of Bouwens et al. 2012). At any given redshift this is obtained by integrating over the distribution of  $\beta$  and using IRX- $\beta$  relationship for a given limiting magnitude. In our model B, we adopt the average  $\eta$  for a limiting magnitude of  $M_{AB} = -16$  and this is given in Table 1. From Fig. 1 and Table 1 it is clear that the dust correction at  $z = 3$  is at least 1.7 times higher than that at other redshifts. This has interesting implications to the redshift evolution of  $f_*$  estimated as we see below.

We found that the LF predictions of model A compares well with observations when suppression due to feedback as described above is applied over  $35 \leq v_c$  ( $\text{km s}^{-1}$ )  $\leq 110$  (or  $v_c^m$  is taken to be  $110 \text{ km s}^{-1}$ ). The radiative feedback is not known to operate in halos with circular velocity greater than  $95 \text{ km s}^{-1}$  (Bromm & Loeb 2002). Therefore, the requirement for suppression of SFR in halos with  $v_c \geq 95 \text{ km s}^{-1}$  could be a signature of the presence of additional feedback mechanisms such as supernovae feedback operating in these galaxies. On the other hand, for model B, we only need the fiducial feedback as given by Bromm & Loeb (2002) to get a reasonable fit to the LFs of LBGs.

Given the above model parameters the remaining crucial parameter  $f_*$ , the fraction of baryons being converted into stars over the life time of the galaxy, is fixed by fitting the observed luminosity function of LBGs using  $\chi^2$  minimization. We note that if we did not have an estimate of  $\eta$  as above, we would only be able to determine the ratio  $f_*/\eta$  as in SSS07. In this manner, our physically motivated model finds the relationship between the halo mass ( $M$ ) and the luminosity ( $L$ ) of the galaxy it hosts. In Fig. 2, we compare the LF predictions in the redshift range 3 – 8 by both models A (in solid black lines) and B (in dotted red lines) with the observed data. The  $f_*$  and reduced  $\chi^2$  obtained by comparing our model predictions with the observed data at various redshifts are tabulated in Table 1. From the figure, it is clear that, the number density of brightest galaxies ( $M_{AB} < -20$ ) as predicted by model A drops faster than that of model B for  $z \geq 5$ . However, both our models compare very well with the observed UV LF of LBGs given by Reddy et al. (2008) for  $z = 3$  and Bouwens et al. (2007) for  $z = 4 - 8$ .

The best fit  $f_*$  for model A (shown in Fig. 2) are 0.34, 0.24, 0.19, 0.23, 0.20 and 0.19 respectively for  $z = 3 - 8$ . For model B, where we use the luminosity independent  $\eta$  the corresponding values of  $f_*$  are 0.46, 0.23, 0.17, 0.16, 0.17 and 0.20. In the middle panel of Fig. 1 we show the  $1\sigma$  range (corresponding to  $\Delta\chi^2 = 1$ ) of  $f_*$  as a function of redshift for model A in shaded black (dark) region and for model B in shaded red (grey) region. The best fit values of  $f_*$  are also tabulated in Table 1.

From Table 1 and Fig. 1, it is clear that,  $f_*$ , the fraction

of baryons being converted into stars, shows only a minor evolution from  $z = 8$  to 4 in both our models. On the other hand, at  $z = 3$ ,  $f_*$  is roughly 1.7 times larger than that at higher redshifts. To understand this, we note that our models predict a nearly constant light to mass ratio ( $f_*/\eta$ ), at all redshifts. But the dust extinction,  $\eta$ , at  $z = 3$  is roughly 2 times the dust extinction in the redshift range 4 – 8 (see left panel of Fig. 1 and Table 1). Thus  $f_*$  is significantly higher at  $z = 3$  compared to best fit  $f_*$  at other redshifts. This implies that the fraction of baryons converted into stars shows a modest evolution in the redshift range 8 – 4, but subsequently increases faster from  $z = 4$  to 3.

On the other hand, SFR in galaxies at any redshift roughly scales as  $f_*/t_d$ , where  $t_d$  is the dynamical time scale at that redshift. We have plotted the  $1\sigma$  range of  $f_*/t_d$  in the right panel of Fig. 1 as a function of redshift for model A in shaded black region (dark) and for model B in shaded red region (grey). From the figure it is clear that  $f_*/t_d$  in dark matter halos shows no significant evolution from  $z = 8$  to 3 which suggest that SFR of galaxies do not change considerably in this time period. This in turn implies that the evolution of dark matter halo mass function can account for the redshift evolution of global star formation rate density of LBGs from  $z = 8$  to 3 without requiring any redshift dependent efficiency of converting baryons into stars which is consistent with previous studies (Tacchella et al. 2013; Behroozi et al. 2013a).

## 4 THE STAR FORMATION HISTORY OF LBGs

In this section, using  $f_*$  values given in Table 1 as a function of  $z$ , we compute  $M_*$  and sSFR of LBGs. Unlike the LFs, these parameters are derived from the observations using SED fitting technique that assumes IMF, star formation history, dust and metallicity. It should be noted that there are strong degeneracies between these parameters (Bouwens et al. 2012; Mitchell et al. 2013; Finlator et al. 2007a; Schaerer et al. 2013), especially when small number of photo metric points are used in the SED fitting.

While we use an IMF similar to what is used in SED fitting analysis, the star formation history in our models is different from those typically used in the SED fitting analysis. Further, when modelling stellar mass functions we incorporate systematic uncertainties in the  $M_*$  due to the typical assumptions about dust, metallicity etc in the SED fitting analysis (Mitchell et al. 2013). A systematic exploration of uncertainties in the dust extinction and derived  $M_*$  due to the effect of various degenerate parameters on SEDs of galaxies is outside the scope of the present work. Therefore, while comparing the model predictions with those derived from SED fitting methods, our main emphasis is to compare the overall trends and not to get exact matching of absolute values.

### 4.1 The $M_{AB}$ - Stellar Mass relationship.

It is clear from Eq. 3 that the  $M_*$  of galaxies in our models are directly proportional to the halo mass. Since the average UV luminosity of galaxies also increases with their mass, we

$z$ (1)	$\beta$ (2)	$d\beta/dM_{AB}$ (3)	Model A			sSFR (7)	$\eta$ (8)	$f_*$ (9)	Model B		
			$f_*$ (4)	$\chi^2_\nu$ (5)	sSFR (6)				$\chi^2_\nu$ (10)	sSFR (11)	sSFR (12)
3	-1.769	-0.166	0.34	0.56	0.96	1.55	3.7	0.46	0.87	0.92	1.44
4	-1.886	-0.113	0.24	1.01	1.89	1.84	2.2	0.23	0.76	1.80	1.75
5	-1.920	-0.130	0.19	1.60	3.20	2.68	2.1	0.17	1.07	3.16	2.81
6	-2.013	-0.191	0.23	0.79	4.48	4.10	1.6	0.16	0.87	4.23	4.22
7	-2.040	-0.180	0.20	0.50	5.60	5.72	1.5	0.17	0.36	4.36	5.76
8	-2.150	-0.130	0.19	0.72	6.40	7.31	1.2	0.20	1.01	3.60	7.31

**Table 1.** Parameters and predictions of our models. Column (1) redshift; columns (2) and (3) the UV-continuum slope  $\beta$  and  $d\beta/dM_{AB}$  at  $M_{AB} = -19.5$  which is used to compute the dust extinction for model A; columns (4) and (9)  $f_*$  for models A and B; columns (5) and (10) reduced  $\chi^2$  obtained for model A and B; columns (6) and (11) sSFR at  $5 \times 10^{10} M_\odot$  predicted by model A and B; columns (7) and (12) sSFR at  $10^{10} M_\odot$  predicted by model A and B; column (8) average dust extinction used in model B;

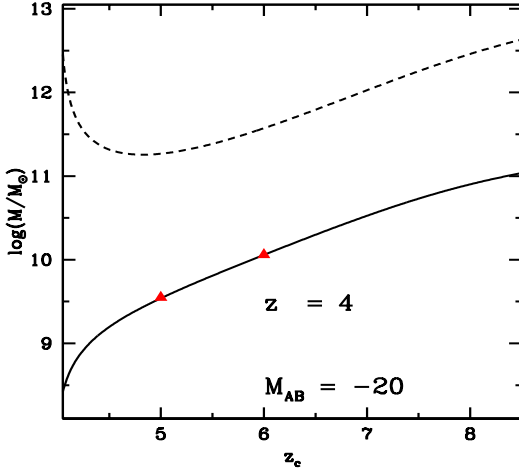


**Figure 3.** The stellar (solid line) and dark matter (dashed line) halo masses of galaxies that shine with  $M_{AB} = -20$  at  $z = 4$  as a function of their formation (collapse) redshift  $z_c$ . The red triangles show the  $M_*$  in galaxies formed at  $z = 5$  and  $6$  and are respectively  $3.4 \times 10^9 M_\odot$  and  $1.1 \times 10^{10} M_\odot$ .

expect correlation between  $M_*$  of galaxies and their luminosities. Further, galaxies of a given absolute magnitude are hosted by dark matter halos of different masses collapsed at different redshifts. At the time of observations these galaxies can have various  $M_*$  depending on their halo mass and collapse redshift (or age). Therefore, galaxies of a given absolute magnitude can have a scatter in their  $M_*$ . This is apparent from Fig. 3, where we have plotted the  $M_*$  and halo mass of galaxies which shine with an absolute magnitude  $M_{AB} = -20$  at  $z = 4$  against their redshift of formation ( $z_c$ ). The solid black line shows the  $M_*$  and the dashed black line shows the halo masses of these galaxies as a function of  $z_c$ . The figure clearly shows that, in our models, galaxies of a given  $M_{AB}$  observed at any  $z$ , will have larger  $M_*$  if they collapsed earlier (larger  $z_c$ ). For example, one can see from Fig. 3 that, for observed  $M_{AB} = -20$  at  $z = 3$ , the  $M_*$  of galaxies that are formed at  $z_c = 5$  is  $3.4 \times 10^9 M_\odot$  whereas the  $M_*$  of a galaxy with  $z_c = 6$  is  $1.1 \times 10^{10} M_\odot$ . These masses are shown in red triangles.

We compute the mean  $M_*$  of galaxies of a given  $M_{AB}$  at any  $z$  as

$$\langle M_*(M_{AB}, z) \rangle = \frac{\int_z^\infty dz_c M_*(M, z_c) \frac{d^2 n}{dM dz_c}(M, z_c)}{\int_z^\infty dz_c \frac{d^2 n}{dM dz_c}(M, z_c)}. \quad (9)$$

Here,  $M_*$  is given by Eq. 3 and  $M = M(M_{AB}, z, z_c)$  is the mass of the dark matter halo that has formed at  $z_c$  and hosting a galaxy which shines with brightness  $M_{AB}$  at  $z$ . In the first three panels of Fig. 4, we show the predictions of mean  $M_*$  in solid black lines for model A with luminosity dependent  $\eta$  at various redshifts as a function of their absolute magnitude at  $1500 \text{ \AA}$ . The dotted red curves are the predictions of mean  $M_*$  for model B with luminosity independent  $\eta$ . Because of the scatter in  $M_*$  at a given magnitude, we also show in Fig. 4, the  $1\sigma$  (68.4%) dispersion in  $M_*$  around its mean value. The data points (solid circles) are the mean  $M_* - M_{AB}$  relation derived using SEDs at  $z = 3$  by Reddy et al. (2012) and at  $z = 4$  and  $5$  by Lee et al. (2012).

We note from Fig. 4 that the predicted trend of  $M_* - M_{AB}$  relations at  $z = 3 - 5$  matches with the observed data of Reddy et al. (2012) and Lee et al. (2012) within the  $1\sigma$  range. The slopes of  $M_* - M_{AB}$  relation as predicted by our models are comparable to the ones given by these authors. For example, at  $z = 4$  Lee et al. (2012) fits their  $M_* - M_{AB}$  with a double power with bright end slope of  $-0.414$  for galaxies brighter than  $M_{AB} = -20.45$ . Our theoretical predictions follow a single power law with slopes  $\sim -0.41$  for model A and  $\sim -0.35$  for model B. On the other hand, González et al. (2011) derived a single power law slope of  $-0.68$  for the  $M_* - M_{AB}$  but with a large standard deviation of  $0.5$  dex around the best fit  $M_*$ . Their scaling relations are in general consistent with the findings of Lee et al. (2012) and hence with our model predictions as well. The  $M_{AB} - M_*$  relations obtained from our models are also consistent with many of the current observations by Stark et al. (2009); González et al. (2010, 2014).

We also show in the last panel of Fig. 4, the mean  $M_*$  of LBGs as a function of their  $M_{AB}$  for  $3 \leq z \leq 8$ . Many of the earlier studies (González et al. 2010, 2014; Lee et al. 2012) find little evolution in the  $M_{AB} - M_*$  relation with redshift. However, Stark et al. (2013) found that the effect of nebular emission in the SEDs of high- $z$  LBGs decreases the derived  $M_*$  for  $z \geq 5$ . They showed that, this will ten-

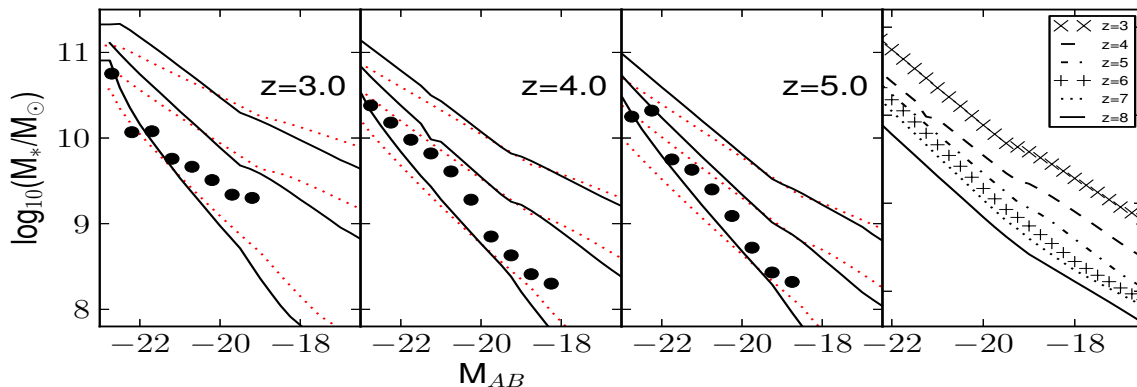


**Figure 4.** First three panels from the left show the mean  $M_*$  of LBGs as a function of their absolute AB magnitudes for three independent redshifts along with the  $1\sigma$  (68.4%) dispersion in  $M_*$  around its mean value. The solid black curves are for model A and red dotted curves are for model B. The observed data points are from Reddy et al. (2012) at  $z = 3$  and from Lee et al. (2012) at  $z = 4$  and 5. The right most panel shows the mean  $M_*$  of LBGs as a function of their  $M_{AB}$  at various redshifts.

tatively result in the evolution of the  $M_* - M_{AB}$  relations with redshift. From their analysis they find a decrease in the overall normalization of the  $M_* - M_{AB}$  relation by a factor of 1.4 – 2.5 in the redshift range 4 to 7. Interestingly our models also predict a decrease in the overall normalization of the  $M_* - M_{AB}$  relation by a factor  $\sim 3$  in the above mentioned range. Stark et al. (2013) further noted that the reduction in the normalization of the  $M_* - M_{AB}$  relation for  $z \geq 5$  is crucial for obtaining a redshift evolution of the derived sSFR as predicted by many theoretical studies.

Finally, we note that the mean  $M_*$  predicted by our models at given magnitude are systematically higher than the predictions of Reddy et al. (2012) and Lee et al. (2012). This could be due to the uncertainties associated with (i) the  $M_*$  of individual galaxies predicted by our model using  $f_*$  which is prone to systematic uncertainties discussed earlier and (ii) the  $M_*$  derived by Reddy et al. (2012); Lee et al. (2012) using SED fitting analysis. The exponentially increasing and constant SFHs used respectively by Reddy et al. (2012) and Lee et al. (2012) for SED fitting analysis can result in significant decrease in inferred  $M_*$  compared to the  $M_*$  inferred using SFH in our models (Finlator et al. 2007a; Schaerer et al. 2013).

## 4.2 The stellar mass functions

The stellar mass function,  $\Phi(M_*, z)$ , is the number density of galaxies of a given  $M_*$  at a given redshift,  $z$ . It can be computed as

$$\Phi(M_*, z) dM_* = \int_z^\infty \frac{d^2 n}{dM dz_c}(M, z_c) dz_c \frac{dM}{dM_*} dM_*. \quad (10)$$

Here the halo mass  $M = M(M_*, z_c)$  is related to the  $M_*$  by Eq. 3. We show our model predictions of stellar mass functions in Fig. 5 for  $z = 3 - 6$ . We also show in this figure, the data of Mortlock et al. (2011) at  $z = 3$  and González et al. (2011); Lee et al. (2012) at other redshifts. Here, our basic model predictions with luminosity dependent dust correction (model A) are shown in solid-black lines. The red-dotted lines show predictions of our model B with constant dust extinction. While computing the stellar mass functions at each redshift, we consider only those galaxies with  $M_{AB} \leq -15$ ,

which is the luminosity selection criteria of González et al. (2011).

We firstly note that our model predictions of stellar mass functions flattens at low mass end rather than being a power law. This flattening is due to the feedback operating in the low mass galaxies and the magnitude threshold criteria used for the galaxy sample. Both our models produce almost identical stellar mass functions with model A producing slightly higher number density of galaxies at the high  $M_*$  end. In general our model predictions compare reasonably well with the observed stellar mass functions of Mortlock et al. (2011) at  $z = 3$  for  $M_* \leq 10^{10} M_\odot$  and with that of González et al. (2011); Lee et al. (2012) for  $M_* \leq 10^9 M_\odot$  at other redshifts. However, we note that they systematically underpredict stellar mass functions typically for  $M_* \geq 10^{10} M_\odot$ . The discrepancy between observationally derived stellar mass functions and theoretical predictions increases with increasing redshift as well. This apparent deficiency in our models could be due to a number of reasons which we will discuss now.

First, the different SFHs used for SED fitting analysis would give different  $M_*$  for the galaxies observed. Schaerer et al. (2013) showed that the constant SFH used by González et al. (2011) for their analysis systematically predicts a larger  $M_*$  compared to the SFH used by our models. Earlier studies of Finlator et al. (2007b) suggested that the differences between  $M_*$  obtained via SEDs when one uses different SFHs are typically less than 0.3 dex. Using simulations and after considering the effects of dust, age, SFH and photometric uncertainties in SEDs, Lee et al. (2012) found that,  $M_*$ , on average, can be recovered within 0.1 dex for LBGs. de Barros et al. (2014) and Stark et al. (2013) found that not incorporating nebular emissions in the SEDs of high- $z$  LBGs also systematically overpredicts  $M_*$  for LBGs at high redshift. The data presented by Mortlock et al. (2011); González et al. (2011); Lee et al. (2012) do not consider the effects of nebular emission. All of these effects discussed above will result in a shift in the observed stellar mass functions to the high mass end.

More importantly, due to various systematic uncertainties, the SED fitting analysis do not recover the true  $M_*$  of the observed galaxies accurately. They rather result in a distribution of the recovered  $M_*$  around the true value of  $M_*$



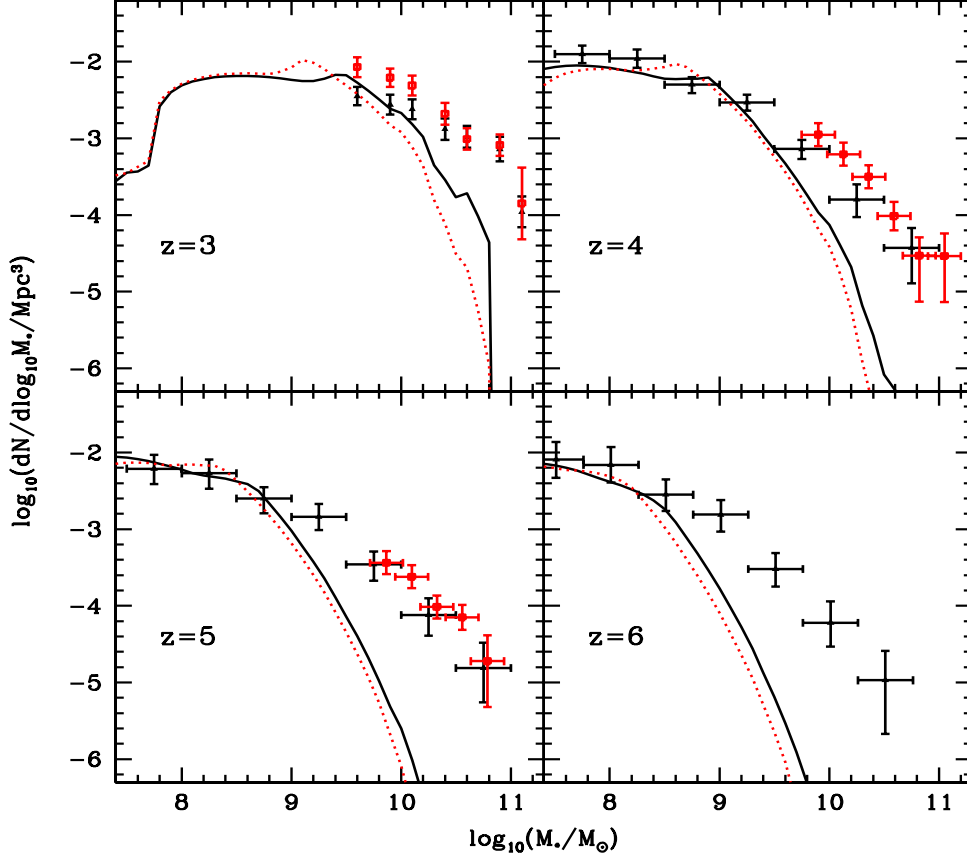


**Figure 5.** The stellar mass functions as predicted by our models from redshifts 3 to 6. The predictions of model A and model B are respectively shown in solid-black red-dotted lines. The data points and error bars are from (i) Mortlock et al. (2011) in black triangles for  $z = 3 - 3.5$  and in red squares for  $z = 2.5 - 3$ , (ii) González et al. (2011) in black triangles for  $z = 3$  to 6 and (iii) Lee et al. (2012) in red squares for  $z = 4$  to 5.

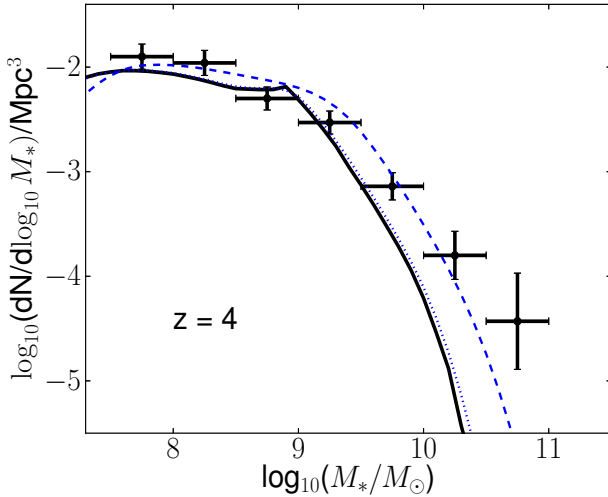


**Figure 6.** The effect of scatter in  $M_*$  in our model predictions of stellar mass functions at  $z = 4$ . The predictions of the model with luminosity dependent  $\eta$  is given in solid black lines. The blue dotted and dashed lines are our model predictions of stellar mass functions which assumes a Gaussian distribution of variance 0.1 and 0.3 dex respectively in the  $M_*$ .

of galaxies (Lee et al. 2012; Schaerer et al. 2013; Mitchell et al. 2013). Such a scatter is evident from Fig. 5 of Lee et al. (2012) where the authors have considered effects of age, dust, SFH and uncertainties related to photometry on SEDs. Schaerer et al. (2013) also show in Fig. 4 of their paper that such a scatter in  $M_*$  is expected when one uses different star formation models.

In particular, Mitchell et al. (2013) have shown how the  $M_*$  obtained by fitting SEDs is affected by the typical assumptions about SFH, metallicity, dust extinction etc in the population synthesis models (See also, Moster et al. 2013). Various SED fitting studies assume fixed values of metallicity and dust for a given type of galaxies whereas in real galaxies these quantities vary stochastically. Mitchell et al. (2013) showed that such assumptions about metallicity and dust in the SED fitting analysis will result in a large scatter in the SED derived  $M_*$  around the true value of  $M_*$ . More interestingly the scatter in the derived  $M_*$  increases with increase in the true  $M_*$  of galaxies and also with the redshift of observation. Thus the observationally derived stellar masses of high mass galaxies are much more sensitive to systematic uncertainties compared to that of low mass galaxies. For example at  $z = 4$  and  $M_* \sim 10^{10} M_\odot$ , the typical scatter in  $M_*$  can be as large as 0.5 dex whereas on smaller mass scales



like  $10^8 M_\odot$  the scatter in  $M_*$  is  $\sim 0.1$  dex. This important effect results in so called Eddington bias (Eddington 1913, 1940) in the observed stellar mass functions, where many low mass galaxies are up scattered to the high mass end.

We have investigated the effect of Eddington bias in our model predictions of stellar mass functions, due to the scatter in the recovered  $M_*$  compared to the true  $M_*$ . To do this we assumed that the stellar mass function at any recovered  $M_*$  has contributions from all the other intrinsic  $M_*$  because of the above mentioned scatter. For simplicity, we have assumed that this scatter is given by a Gaussian distribution of variance  $\sigma_{\log M_*}$  dex. Assuming  $M'_*$  to be the true stellar mass and  $M_*$  to be the recovered stellar mass, the modified stellar mass function ( $\Phi_G$ ) after taking care of the Eddington bias can be computed from the actual stellar mass function ( $\Phi$ ) as

$$\Phi_G(M_*) = \int dM'_* \Phi(M'_*) \frac{1}{\sqrt{2\pi\sigma_{\log M_*}^2}} \exp \left[ -\frac{1}{2} \left( \frac{\log(M'_*) - \log(M_*)}{\sigma_{\log M_*}} \right)^2 \right]. \quad (11)$$

In Fig. 6, we demonstrate the effect of Eddington bias on stellar mass functions. Here the solid black curve corresponds to predictions of model A with luminosity dependent dust correction ( $\sigma_{\log M_*} = 0$ ). In this figure we also show the modified stellar mass function  $\Phi_G(M_*)$  for models with  $\sigma_{\log M_*} = 0.1$  and 0.3 dex in dotted and dashed blue lines. The models with  $\sigma_{\log M_*} = 0.1$  dex do not alter stellar mass functions appreciably. Since the scatter in derived  $M_*$  are small for low  $M_*$  we expect the low mass end of the stellar mass functions to be not affected by the Eddington bias. On the other hand, a scatter of 0.3 dex in the  $M_*$  considerably changes the slope of stellar mass functions at high mass end and better represent the observed data. Also, as already mentioned, the scatter in the  $M_*$  derived from SEDs are much larger for high  $M_*$ . We further note that, the stellar mass function has a steep fall at the high stellar mass end. Therefore, even a constant error across all masses will widen the distribution, thereby enhancing the number of inferred galaxies at the high stellar mass end. Therefore, we conclude that effect of Eddington bias is important while modelling high redshift LBG stellar mass functions and that our models are consistent with the data within the allowed Eddington bias.

### 4.3 The specific star formation rate

In our model, even though the sSFR of galaxies forming at a given redshift is independent of the halo mass  $M$  (see Eq. (4)), the total  $M_*$  in them can differ, depending on the mass of the hosting dark matter halo. Conversely, galaxies of different sSFR (forming at different redshifts), can have the same  $M_*$  depending on their dark matter halo mass. The average sSFR at redshift  $z$  of galaxies of a given  $M_*$  is given by

$$sSFR(M_*, z) = \frac{\int dz_c sSFR(M, z_c) \frac{dn(M, z_c)}{dz_c} \frac{dM}{dM_*}}{\int dz_c \frac{dn(M, z_c)}{dz_c} \frac{dM}{dM_*}}, \quad (12)$$

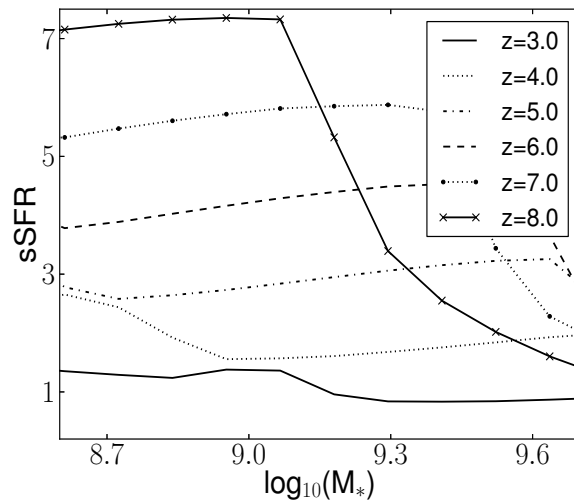


**Figure 7.** The mean sSFR computed using Eq. (12) as a function of  $M_*$  at different redshifts.

where halo mass  $M = M(M_*, z_c)$  is related to the  $M_*$  by Eq. 3 and  $sSFR(M, z_c)$  is given by Eq. (4). In Fig. 7 we show the mean sSFR of galaxies as a function of their  $M_*$  for  $3 \leq z \leq 8$ . One can clearly see from the figure that for  $5 \times 10^8 \leq M_*/M_\odot \leq 5 \times 10^9$  the sSFR is nearly constant for redshift range  $z = 3 - 7$ . Similar trend has been noted at  $z = 2.3$  by the observational studies of Reddy et al. (2012) as well. For highest redshift galaxies (i.e  $z \sim 8$ ), our models predict a sharp decrease in the mean sSFR for  $M_* \geq 10^9 M_\odot$ .

One particular quantity of interest is the sSFR at a fixed  $M_*$ . We have over plotted mean sSFR in Fig. 8 at  $M_* = 5 \times 10^9 M_\odot$  and  $10^9 M_\odot$  as a function of redshift along with the observationally derived sSFR by various authors. The black solid line is the prediction of our model A whereas the red dotted line is for model B. These curves are obtained after averaging the sSFR of galaxies in mass bins centered around the specified  $M_*$  and of width 0.3 dex. (See figure description for details about observed data). Since sSFR is not a strong function of  $M_*$  for  $5 \times 10^8 \leq M_*/M_\odot \leq 5 \times 10^9$ , we expect that the uncertainties in  $M_*$  from SED fitting analysis will not strongly affect the mean sSFR at  $M_* = 10^9 M_\odot$ . Thus mean sSFRs of galaxies at this mass scale ( $10^9 M_\odot$ ) is a more robust quantity than stellar mass functions for constraining galaxy formation physics. We have also tabulated these mean sSFR in Table 1.

The evolution of sSFR with redshift has been studied extensively in the literature, both observationally (Feulner et al. 2005; Reddy et al. 2012; Stark et al. 2009; Bouwens et al. 2012; González et al. 2014) and theoretically (Bouché et al. 2010; Weinmann et al. 2011; Krumholz et al. 2012; Behroozi et al. 2013b). Many of the theoretical studies suggest a rapid evolution of sSFR with redshift as  $(1+z)^{2.4}$  (Bouché et al. 2010; Weinmann et al. 2011; Krumholz et al. 2012). In contrast, earlier observational evidence suggested a nearly flat plateau for the sSFR for  $z > 3$  (Stark et al. 2009; González et al. 2010). However most recent studies, including the effects of luminosity dependent dust obscuration and nebular emission in the SED fitting showed that sSFR does evolve with redshift (Bouwens et al. 2012; González et al. 2014). In the case of model A incorporating the luminosity dependent dust extinction mean sSFR at  $M_* = 5 \times 10^9 M_\odot$

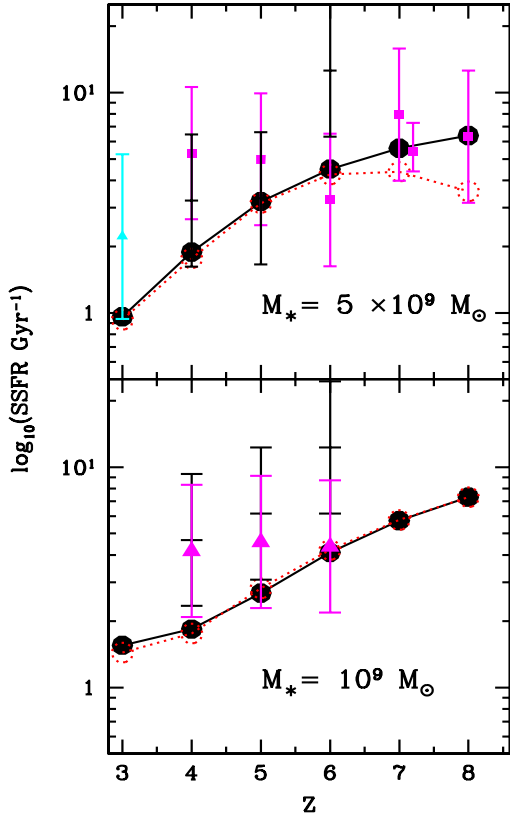


**Figure 8.** Top panel: The mean sSFR at  $M_* = 5 \times 10^9 M_\odot$  as predicted by our models as a function of redshift. The data points and error bars are from (i) Feulner et al. (2005) ( $z = 3$ , yellow-line) (ii) Reddy et al. (2012) ( $z = 3$ , green, triangle) (iii) Stark et al. (2009) ( $z = 4 - 6$ , cyan, hexagon) (iv) Bouwens et al. (2012) ( $z = 4 - 8$ , magenta, square) and (v) González et al. (2014) ( $z = 4 - 8$ , black, line). Bottom panel: The mean sSFR at  $M_* = 10^9 M_\odot$ . The observed data are given by González et al. (2014) for rising (black, line) and constant (magenta, triangle) star formation models. In both panels, the solid black-curves are predictions of model A with luminosity dependent  $\eta$  whereas the red-dotted lines are the predictions of model B with luminosity independent  $\eta$ .

evolves as  $(1+z)^{2.4}$  over the redshift range  $3 \leq z \leq 8$  which is in agreement with most of the theoretical studies. In our model B with luminosity independent  $\eta$ , the mean sSFR increases as  $(1+z)^{1.9}$  for  $3 \leq z \leq 7$ . In general, sSFR at  $M_* = 5 \times 10^9 M_\odot$  as predicted by our models compares well with the observationally derived sSFR within  $1\sigma$  limits. For galaxies with  $M_* = 10^9 M_\odot$ , both our models A and B predict the evolution of sSFR as  $(1+z)^2$ .

## 5 CONCLUSIONS

We have extended our physically motivated model to understand the evolution of  $M_* - M_{AB}$  scaling relations, stellar mass functions and sSFR of LBGs along with their UV luminosity functions in the redshift range  $3 \leq z \leq 8$ . In our model, galaxies are assumed to be formed in dark matter halos by continuous star formation which is proportional to

the halo mass and extending over a period of a few dynamical time scales of the halo. This SFR combined with the halo formation rate gives the UV LF of LBGs which is compared with observed UV LF of LBGs to constrain the parameters related to the star formation.

Using the observationally derived dust extinction parameter,  $\eta$ , we have obtained an estimate on  $f_*$ , the fraction of baryons being converted into stars over the lifetime of the galaxy. We found that  $f_*$  is  $\sim 0.2$  to  $0.4$  for LBGs in the redshift range  $8$  to  $3$ , with major evolution occurring between redshifts  $3$  and  $4$ . On the other hand,  $f_*/t_d$ , the parameter that scales as the SFR in LBGs is relatively constant and of order  $\sim 0.2$  for  $3 \leq z \leq 8$ . This important result implies that the rate of conversion of baryons into stars is fairly constant for LBGs in the redshift range  $3 \leq z \leq 8$ . Therefore, during this period, the growth of the global star formation rate density can be explained solely by the evolution of dark matter halo mass function.

Using the value of  $f_*$  determined by fitting the observed UV LF of LBGs, we obtained  $M_*$  of individual halos at any given redshift. This enables us to further compute the correlation between  $M_*$  and UV luminosity of LBGs, their stellar mass functions and sSFR.

We note that our model predictions of  $M_* - M_{AB}$  correlations of LBGs at  $z = 3 - 5$  compare reasonably well with the observed data of Reddy et al. (2012) and Lee et al. (2012). Our models predict a slope of  $\sim -0.40$  for the  $M_* - M_{AB}$  relation which is in good agreement with the bright end slope of this relation derived by Lee et al. (2012) using SED fitting. Further, normalization of the  $M_* - M_{AB}$  relation in our models is found to decrease by a factor 3 in the redshift range  $4 - 7$  which is consistent with the findings of Stark et al. (2013).

The stellar mass functions computed using our models also compares reasonably well with observed data for  $M_* \leq 10^{10} M_\odot$  at  $z = 3$  and for  $M_* \leq 10^9 M_\odot$  at  $z = 4 - 6$ . For higher  $M_*$  our models underpredict stellar mass functions. However, we have shown that this discrepancy could be due to the uncertainties in the  $M_*$  derived using SED fitting technique. Mitchell et al. (2013) showed that assumptions about dust, metallicity etc., will result in a scatter in the the observationally derived  $M_*$  around it's true value. Further the uncertainty in the derived  $M_*$  increases with increase in the true  $M_*$  of the galaxy. We found that applying such a scatter in our theoretical models will up scatter many of the low stellar mass galaxies to the high mass end, significantly improving the agreement of our model predictions with observed data. Thus we conclude that, the systematic uncertainties in the derived  $M_*$  should be accounted for while comparing theoretical models of stellar mass functions to observed data to constrain galaxy formation physics.

We found that the sSFR of galaxies in our models at a given redshift is not a strong function of their  $M_*$  for  $5 \times 10^8 \leq M_*/M_\odot \leq 5 \times 10^9$ , thus making it a much more robust quantity to constrain the physics of galaxy formation as compared to stellar mass functions. The sSFR computed using our models at  $M_*$  of  $5 \times 10^9 M_\odot$  and  $10^9 M_\odot$  compares well with the observed data. Our models with luminosity dependent dust extinction predict that sSFR at  $5 \times 10^9 M_\odot$  evolves as  $(1+z)^{2.4}$  for  $3 \leq z \leq 8$  which is in agreement with previous theoretical studies. At  $10^9 M_\odot$  the sSFR increases as  $(1+z)^2$ . In general our findings are consistent the sSFR

derived by (Bouwens et al. 2012; González et al. 2014) using SED fittings within  $1\sigma$  limits even though the authors find only a moderate evolution in the mean sSFR with redshift.

In summary our physically motivated model presented in this paper explains various observables related to LBGs derived using SED fitting analysis along with their UV LFs. Remarkably, the key ingredient of this model, SFR in LBGs, extending for a dynamical time scale of the hosting dark matter halos shows no significant evolution for  $3 \leq z \leq 8$ . This evidently suggest that, the build up dark matter halos over the first two gigayears of the cosmic expansion, without invoking any redshift dependent efficiency of star formation activity in them, is sufficient to explain key observables related to LBGs.

Possible improvements to our work include exploring other forms of star formation histories in individual halos, and/or using merger trees instead of the halo formation rate prescription that we have used. However this will entail reproducing all the observables including the UV LFs and clustering of LBGs and LAEs, that our present model successfully explains.

## ACKNOWLEDGMENTS

We thank Peter Behroozi for providing the observed data of stellar mass functions and sSFR. CJ acknowledges support from CSIR. CJ acknowledges support from CSIR. We also thank the referee for the useful comments that helped us to improve the paper.

## REFERENCES

- Adelberger K. L., Steidel C. C., Giavalisco M., Dickinson M., Pettini M., Kellogg M., 1998, *ApJ*, 505, 18
- Beckwith S. V. W. et al., 2006, *AJ*, 132, 1729
- Behroozi P. S., Wechsler R. H., Conroy C., 2013a, *ApJ*, 762, L31
- Behroozi P. S., Wechsler R. H., Conroy C., 2013b, *ApJ*, 770, 57
- Benson A. J., Lacey C. G., Baugh C. M., Cole S., Frenk C. S., 2002, *MNRAS*, 333, 156
- Best P. N., Kaiser C. R., Heckman T. M., Kauffmann G., 2006, *MNRAS*, 368, L67
- Bielby R. M. et al., 2011, *MNRAS*, 414, 2
- Bouché N. et al., 2010, *ApJ*, 718, 1001
- Bouwens R. J. et al., 2009, *ApJ*, 705, 936
- Bouwens R. J., Illingworth G. D., Franx M., Ford H., 2007, *ApJ*, 670, 928
- Bouwens R. J., Illingworth G. D., Franx M., Ford H., 2008, *ApJ*, 686, 230
- Bouwens R. J. et al., 2012, *ApJ*, 754, 83
- Bouwens R. J. et al., 2011, *ApJ*, 737, 90
- Bouwens R. J. et al., 2010, *ApJ*, 709, L133
- Bower R. G., Benson A. J., Malbon R., Helly J. C., Frenk C. S., Baugh C. M., Cole S., Lacey C. G., 2006, *MNRAS*, 370, 645
- Bromm V., Loeb A., 2002, *ApJ*, 575, 111
- Chiu W. A., Ostriker J. P., 2000, *ApJ*, 534, 507
- Choudhury T. R., Srianand R., 2002, *MNRAS*, 336, L27
- de Barros S., Schaerer D., Stark D. P., 2014, *A&A*, 563, A81
- Dijkstra M., Haiman Z., Rees M. J., Weinberg D. H., 2004, *ApJ*, 601, 666
- Eddington A. S., 1913, *MNRAS*, 73, 346
- Eddington, Sir A. S., 1940, *MNRAS*, 100, 354
- Feulner G., Gabasch A., Salvato M., Drory N., Hopp U., Bender R., 2005, *ApJ*, 633, L9
- Finlator K., Davé R., Oppenheimer B. D., 2007a, *MNRAS*, 376, 1861
- Finlator K., Davé R., Oppenheimer B. D., 2007b, *MNRAS*, 376, 1861
- Giavalisco M., Dickinson M., 2001, *ApJ*, 550, 177
- Giavalisco M. et al., 2004, *ApJ*, 600, L93
- Gnedin N. Y., 1996, *ApJ*, 456, 1
- González V., Bouwens R., Illingworth G., Labbé I., Oesch P., Franx M., Magee D., 2014, *ApJ*, 781, 34
- González V., Labbé I., Bouwens R. J., Illingworth G., Franx M., Kriek M., 2011, *ApJ*, 735, L34
- González V., Labbé I., Bouwens R. J., Illingworth G., Franx M., Kriek M., Brammer G. B., 2010, *ApJ*, 713, 115
- Grogin N. A. et al., 2011a, *ApJS*, 197, 35
- Grogin N. A. et al., 2011b, *ApJS*, 197, 35
- Hildebrandt H., Pielorz J., Erben T., van Waerbeke L., Simon P., Capak P., 2009, *A&A*, 498, 725
- Illingworth G. D. et al., 2013, *ApJS*, 209, 6
- Jose C., Samui S., Subramanian K., Srianand R., 2011, *Phys. Rev. D*, 83, 123518
- Jose C., Srianand R., Subramanian K., 2013a, *MNRAS*, 435, 368
- Jose C., Subramanian K., Srianand R., Samui S., 2013b, *MNRAS*, 429, 2333
- Kashikawa N. et al., 2006, *ApJ*, 637, 631
- Koekemoer A. M. et al., 2011, *ApJS*, 197, 36
- Krumholz M. R., Dekel A., McKee C. F., 2012, *ApJ*, 745, 69
- Larson D. et al., 2011, *ApJS*, 192, 16
- Lee K.-S. et al., 2012, *ApJ*, 752, 66
- Leitherer C. et al., 1999, *ApJS*, 123, 3
- Lorenzoni S., Bunker A. J., Wilkins S. M., Caruana J., Stanway E. R., Jarvis M. J., 2013, *MNRAS*, 429, 150
- Madau P., Ferguson H. C., Dickinson M. E., Giavalisco M., Steidel C. C., Fruchter A., 1996, *MNRAS*, 283, 1388
- McLure R. J. et al., 2013, *MNRAS*, 432, 2696
- Meurer G. R., Heckman T. M., Calzetti D., 1999, *ApJ*, 521, 64
- Mitchell P. D., Lacey C. G., Baugh C. M., Cole S., 2013, *MNRAS*, 435, 87
- Mortlock A., Conselice C. J., Bluck A. F. L., Bauer A. E., Grützbauch R., Buitrago F., Ownsworth J., 2011, *MNRAS*, 413, 2845
- Moster B. P., Naab T., White S. D. M., 2013, *MNRAS*, 428, 3121
- Oesch P. A. et al., 2010, *ApJ*, 725, L150
- Oesch P. A. et al., 2013, *ApJ*, 773, 75
- Oke J. B., Gunn J. E., 1983, *ApJ*, 266, 713
- Ouchi M. et al., 2005, *ApJ*, 635, L117
- Ouchi M. et al., 2004a, *ApJ*, 611, 660
- Ouchi M. et al., 2004b, *ApJ*, 611, 685
- Reddy N. A., Pettini M., Steidel C. C., Shapley A. E., Erb D. K., Law D. R., 2012, *ApJ*, 754, 25
- Reddy N. A., Steidel C. C., 2009, *ApJ*, 692, 778

- Reddy N. A., Steidel C. C., Pettini M., Adelberger K. L., Shapley A. E., Erb D. K., Dickinson M., 2008, *ApJS*, 175, 48
- Samui S., 2014, *New A*, 30, 89
- Samui S., Srianand R., Subramanian K., 2007, *MNRAS*, 377, 285
- Samui S., Srianand R., Subramanian K., 2009, *MNRAS*, 398, 2061
- Samui S., Subramanian K., Srianand R., 2008, *MNRAS*, 385, 783
- Savoy J., Sawicki M., Thompson D., Sato T., 2011, *ApJ*, 737, 92
- Schaerer D., de Barros S., Sklias P., 2013, *A&A*, 549, A4
- Schenker M. A. et al., 2013, *ApJ*, 768, 196
- Sheth R. K., Tormen G., 1999, *MNRAS*, 308, 119
- Stark D. P., Ellis R. S., Bunker A., Bundy K., Targett T., Benson A., Lacy M., 2009, *ApJ*, 697, 1493
- Stark D. P., Schenker M. A., Ellis R., Robertson B., McLure R., Dunlop J., 2013, *ApJ*, 763, 129
- Steidel C. C., Adelberger K. L., Dickinson M., Giavalisco M., Pettini M., Kellogg M., 1998, *ApJ*, 492, 428
- Steidel C. C., Adelberger K. L., Giavalisco M., Dickinson M., Pettini M., 1999, *ApJ*, 519, 1
- Steidel C. C., Giavalisco M., Dickinson M., Adelberger K. L., 1996, *AJ*, 112, 352
- Tacchella S., Trenti M., Carollo C. M., 2013, *ApJ*, 768, L37
- Weinmann S. M., Neistein E., Dekel A., 2011, *MNRAS*, 417, 2737
- Wilkins S. M., Gonzalez-Perez V., Lacey C. G., Baugh C. M., 2012, *MNRAS*, 424, 1522
- Windhorst R. A. et al., 2011, *ApJS*, 193, 27